

Growth mode of ultrathin copper overlayers on $\text{TiO}_2(110)$

U. Diebold, J.-M. Pan, and T. E. Madey

*Department of Physics and Astronomy and Laboratory for Surface Modification,
Rutgers, The State University of New Jersey, P.O. Box 849, Piscataway, New Jersey 08855*
(Received 2 July 1992)

Copper overlayers with thicknesses up to several tens of angstroms have been vapor deposited at various substrate temperatures onto rutile $\text{TiO}_2(110)$ surfaces that have different defect concentrations. The metal films have been studied by means of He^+ low-energy ion scattering, x-ray photoelectron spectroscopy, and LEED (low-energy electron diffraction). Our measurements clearly show that Volmer-Weber growth (formation of three-dimensional crystallites) occurs even at sample temperatures as low as 160 K. Defects created by sputtering the substrate prior to Cu deposition do not influence the subsequent growth of the Cu films. The clusters are oriented with their (111) orientation parallel to the surface as confirmed by LEED. During low-temperature annealing, a coarsening of the crystallites takes place. The size of the clusters and the coverage have been modeled using simple assumptions about their shape. An average thickness of approximately 10 Å is needed to cover half of the sample with Cu. The growth mode can be attributed to a very weak interaction between Cu and the substrate.

I. INTRODUCTION

In recent years, the interaction of metals with metal oxides has been studied with growing interest. The understanding of the metal-metal oxide interface properties is crucial for further developments in the design of new ceramic materials. In heterogeneous catalysis, the dispersion, geometry, and wetting properties of very thin metal films on metal oxides used as support materials is of great interest. By examination of the morphology of ultrathin ($< 50\text{-}\text{Å}$) metal films on well-characterized metal oxides, one can get insights into the nature of the bond between metal and oxide.

The growth modes of vapor-deposited thin films are generally classified as follows, and are named after their original investigators:¹ Franck-van der Merwe (monolayer-by-monolayer growth, FM), Stranski-Krastanov (layer growth up to one or a few monolayers, followed by three-dimensional crystallite growth, SK) and Volmer-Weber (formation of three-dimensional crystallites without a preceding adsorbed layer, VW). These are equilibrium growth modes; the growth may be limited by kinetic factors when films are deposited at conditions far from thermodynamic equilibrium.

The driving force for the appearance of one of the growth types is the minimization of the energy of the system. The growth mode will depend on the surface energy of the substrate and adsorbate, respectively, and on the interfacial energy. Whereas the surface energies can be calculated or determined experimentally, the interfacial energy cannot be obtained easily. Especially in the case of an oxide, chemical interactions between the overlayer metal and the surface oxygen at the interface can complicate the situation. One should also note that the concept of energy minimization in principle only holds in thermodynamic equilibrium and that the appearance of the growth modes may be limited by kinetic factors.

We have chosen TiO_2 as a model substrate for studying

the growth of ultrathin transition-metal oxide films. TiO_2 is widely used as a support material in heterogeneous catalysis. The (110) face is a well-characterized, stable surface, where defects can be introduced in a controlled fashion.² These defect sites are known to be reactive for gas adsorption,³ and might play an important role as nucleation centers during the overlayer formation.

Because Cu is a fairly unreactive metal, only a weak interaction with the surface oxygen can be expected and the simple concept of comparing substrate and surface free energies might be valid. We have found that for $\text{Cu}/\text{TiO}_2(110)$, Volmer-Weber growth takes place at substrate temperatures as low as 160 K, in contrast to the Stranski-Krastanov growth proposed formerly for this system.^{4,5} Even at this low temperature, diffusion takes place and can be observed within the time scale of the experiment. This work is part of a systematic investigation of the growth of different transition metals on $\text{TiO}_2(110)$, where we observe a change in growth mode with an increase of overlayer metal reactivity toward oxygen.^{6,7}

II. EXPERIMENT

The experiments were performed in an UHV chamber with a base pressure of 1×10^{-10} Torr; a detailed description of the equipment can be found elsewhere.⁸ A differentially pumped ion gun (Perkin-Elmer 11-665) was used for cleaning the sample and for low-energy ion-scattering (LEIS) measurements. A VSW HA-100 hemispherical energy analyzer was operated in the fixed retard ratio mode, with the retardation ratio set at five for LEIS. The He^+ ion energy used in LEIS measurements was 1500 eV. The beam was rastered across the front surface of the sample with a current density of about $0.4 \mu\text{A}/\text{cm}^2$. Collecting an individual spectrum took about 3 min; this corresponds to a fluence of 4.5×10^{14} He^+ ions/ cm^2 . Since damage due to sputtering by the probing ion beam accumulates during sequential evaporation

steps,⁹ the results were obtained by averaging over several evaporation runs with varying metal doses. The ion beam was incident on the surface at an angle of 45° from the surface normal, and ions backscattered through 135° were detected with our analyzer.

X-ray photoemission spectroscopy (XPS) was performed using Al $K\alpha$ radiation (photon energy 1486.6 eV) with a fixed pass energy of 44 eV in the hemispherical analyzer ($\Delta E = 1$ eV). The surface normal was usually directed toward the analyzer entrance. During the Cu-evaporation experiments, spectra of the Ti $2p_{3/2}$, O $1s$, and Cu $2p_{3/2}$ lines have been recorded. Routinely, wide region energy scans have been taken to monitor the presence of contaminants on the surface.

Several $10 \times 5 \times 1$ -mm³ polished TiO₂(110) crystals from Commercial Crystal Laboratories were used as samples. The sample was held by a Ta foil holder which provided electrical and thermal contact. High-temperature annealing was accomplished through radiation and electron bombardment from a W filament placed behind the crystal. For annealing to lower temperatures (<400°C), the crystal was not biased with respect to the filament to avoid oxygen desorption from the TiO₂ substrate by electron-stimulated desorption. The temperatures were measured with a W/Re thermocouple spot welded on the Ta foil near the crystal. When the sample was heated, the true sample temperature was believed to be lower than the measured temperature. The thermocouple reading during cooling with liquid nitrogen indicated a temperature of 100 K, but due to the imperfect thermal contact between the Ta holder and the sample, this reading gives the temperature of the holder rather than the correct sample temperature. We estimate the sample temperature during cooling as 160 K, since we were not able to adsorb multilayers of H₂O, but we observed water adsorption on a partly Cu-covered TiO₂(110) surface, which gives an upper limit of 170 K for desorption of H₂O from Cu.¹⁰

After inserting a fresh TiO₂ sample into the vacuum system, it was reduced by a long period of heating in UHV at about 1000 K. Diffusion of oxygen from the bulk and subsequent desorption from the surface resulted in formation of *n*-type semiconducting TiO₂,¹¹ and the sample changed its color from transparent to dark blue. After this initial treatment no charging problems during XPS and LEIS measurements occurred, and the sample could be used for experiments for a long period of time (approximately one-half of a year). The data shown have been obtained using four different crystals, with no difference in results.

Before each measurement, the TiO₂(110) surface was prepared in the following way: First the surface was sputtered with 500-eV Ar⁺, then annealed to 1000 K for 10 min in 2×10^{-6} Torr of O₂, cooled down to room temperature, and exposed for ten more minutes to the same oxygen atmosphere. This resulted in a total oxygen dose of ~ 4000 L. XPS showed sharp Ti $2p$ peaks with no indication of reduced Ti states. We believe that the surface is almost perfectly stoichiometric, since we were able to monitor a defect concentration of ~ 0.03 monolayer (ML) on a purposely slightly damaged surface.⁹ The sur-

face showed a (1 \times 1) low-energy electron-diffraction (LEED) pattern.

To study the influence of defects on the growth mode, the well-annealed stoichiometric surface was sputtered with 500-eV Ar⁺ for 10 min with a sample current of 2 μ A. There were several reduced Ti states observed from XPS. After sputtering, no LEED pattern was observed but the surface was still ordered locally, as seen with medium-energy backscattered electron diffraction (MEED).⁸

Cu evaporation was performed with a home-built evaporation source that consisted of a tungsten filament wrapped with a Cu wire (purity 99.9985%). The Cu was melted initially to improve the thermal contact between the Cu and the W. The temperature of the source was monitored with a Chromel-Alumel (type-K) thermocouple spot-welded onto the W filament. During evaporation, the sample was placed at a distance of ~ 5.5 cm away from the Cu source. No increase of sample temperature was observed during evaporation; the evaporation rate was ~ 1 Å per minute. A typical evaporation step in one of the curves shown below (Fig. 1) took approximately 10 min. This is important to keep in mind since we will show that diffusion of Cu occurs even at low temperature, and each experimental observation will therefore depend on its specific time scale.

A water-cooled quartz-crystal film-thickness monitor (QCM) (LEYBOLD INFICON XTC) was put at the same distance from the Cu source as the sample during evaporation. This was very helpful: since the film thickness could be monitored during evaporation, slight changes in the evaporation rate of the Cu source were not important. The QCM was calibrated by preparing a sample with a thick Cu overlayer and examining it with high-resolution transmission electron microscopy (HRTEM). The HRTEM results will be published sepa-

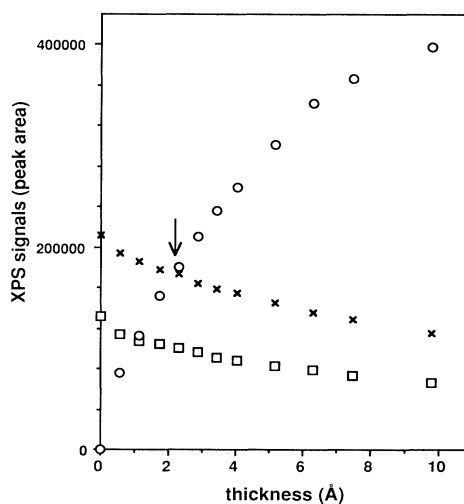


FIG. 1. The XPS spectra of Cu films evaporated onto stoichiometric TiO₂(110) at room temperature. The integrated peak areas of Cu $2p_{3/2}$ (circles), Ti $2p_{3/2}$ (squares), and O $1s$ (crosses) are shown. The arrow indicates the position where a monolayer break would be expected.

rately.¹² Due to the atomic resolution of the micrographs, a very accurate measurement of the Cu film thickness was possible. Based on the HRTEM results, the thickness reading of the QCM was corrected by a factor of 0.85. In the figures shown below, the corrected reading of the QCM is given for the thickness of the Cu films.

In addition, several samples with varying Cu thicknesses ($\sim 15\text{--}30\text{ \AA}$) have been prepared in the UHV chamber and examined by Rutherford backscattering (RBS) in a separate chamber. The RBS measurements showed the same trend as the HRTEM results, $\sim 20\%$ lower thickness than expected from the QCM. The average Cu film thicknesses were quite uniform (a variation of 10%) across the crystal.

III. RESULTS

A. Copper deposition onto TiO_2 at room temperature

A standard method for the determination of growth modes is to use electron spectroscopy, mostly Auger-electron spectroscopy (AES) or XPS, to measure the adsorbate the substrate signals while increasing the exposure of the overlayer metal.¹³ The S - t plots (electron spectroscopy signal versus evaporation time, or any other signal which is related to the average film thickness) should have a characteristic shape depending on the growth mode of the adsorbate metal: A completion of a full monolayer is expected to be manifested in a distinct change in the slopes (a "break") in both the substrate and overlayer signals. In case of FM growth, for example, the S - t curves should consist of straight-line segments with decreasing slope. The growth of three-dimensional crystallites (Volmer-Weber growth, VW) or simultaneous multilayer growth should give rise to a smooth increase of overlayer and decrease of substrate signals, respectively.

No clear breaks can be observed in the XPS signals for Cu evaporation onto a stoichiometric $\text{TiO}_2(110)$ surface at room temperature (Fig. 1). The method of S - t curves has been applied with success by several investigators using XPS and AES,¹³ but scatter in the data and change in line shapes can make the assignment and interpretation of breaks difficult. Although the data are consistent with a VW growth mode, we believe that the absence of breaks in the S - t curve alone (Fig. 1) is not conclusive evidence for the assignment of any growth mode.

A much stronger indication for VW growth of Cu on $\text{TiO}_2(110)$ at room temperature comes from the low-energy ion-scattering (LEIS) spectra shown in Fig. 2. LEIS with He^+ ions is an extremely surface-sensitive method with virtually no signal contributed by the second or deeper layers of a surface. This makes it a unique tool for the determination of growth modes, especially for distinguishing between modes where the adsorbate initially wets the surface (FM or SK), and the VW growth mode, where three-dimensional crystallites or clusters are formed from the very first stages of the evaporation process. In the case of VW growth, a contribution from the substrate is expected to be visible in the spectra up to quite high coverages, as is observed in Fig.

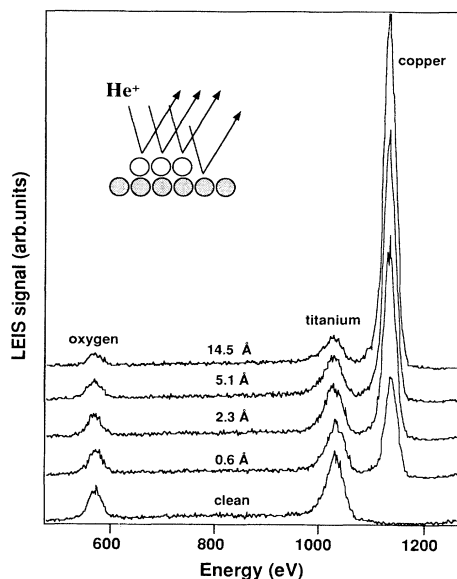


FIG. 2. The low-energy He^+ ion-scattering spectra of Cu evaporated onto stoichiometric $\text{TiO}_2(110)$ at room temperature. The thickness of the Cu film is indicated, the primary energy of He^+ was 1.5 keV, and the scattering angle 135° .

2. The relative intensity of the Cu signal in the LEIS spectra is much higher than of the substrate (oxygen and titanium), due to different scattering cross sections and, possibly, to neutralization effects. However, at coverages well below one monolayer, substantial contributions due to backscattering of He^+ from substrate atoms are visible. [One monolayer would correspond to an average thickness of 2.09 \AA , assuming (111) orientation of the Cu overlayer, see below.]

With LEIS, one cannot distinguish between FM and SK growth. In the simplest case, the adsorbate signal should increase linearly with coverage and the substrate signal should show a linear decrease.^{14,15} As soon as the first monolayer is completed, the substrate signal is expected to decrease to zero and the adsorbate signal to remain constant. For VW growth, the substrate as well as the adsorbate signals should be smooth functions of the adsorbate coverage. Figure 3 shows the integrated peak area of the substrate LEIS intensities, normalized to the intensity of clean spectra. Both the oxygen and titanium signals decrease in the same way within the uncertainty of the data. This was observed also for very low coverages, well below an average thickness of one monolayer (not shown in Fig. 3).

The intensity of the signals depends on the size, shape, and distribution of the crystallites, and to a first approximation (assuming constant neutralization probabilities and no macroscopic shadowing) at least 30% of the substrate is still uncovered at a film thickness as high as 30 \AA .

In a previous study of the geometrical and electronic structure of ultrathin Cu overlayers on $\text{TiO}_2(110)$, the initial growth mode was reported as Stranski-Krastanov type.^{4,5} In this study, Auger-electron spectroscopy was

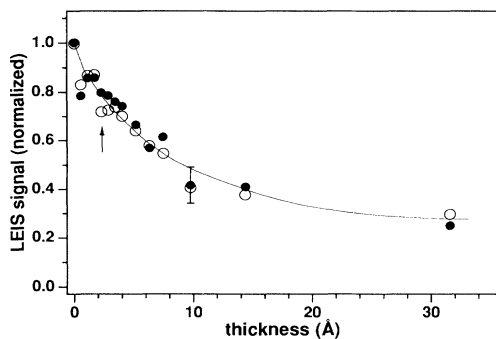


FIG. 3. The low-energy ion-scattering signal of oxygen (open circles) and titanium (dark circles) of Cu evaporated onto stoichiometric $\text{TiO}_2(110)$ at room temperature. The line is drawn to guide the eye. The arrow indicates the Cu thickness which would correspond to one monolayer.

employed for the determination of the growth mode; because of the above-mentioned difficulties in the assignment of breaks in S - t curves, we believe that our determination of Volmer-Weber growth using LEIS is a more reliable result.

As already discussed in Ref. 4, the Cu clusters show a slightly contracted (111) structure at higher coverages, commensurate along the $[1\bar{1}0]$ direction of the substrate. We observe a faint hexagonal LEED pattern above a nominal overlayer thickness of ~ 15 Å, together with a (1×1) substrate pattern. The overlayer LEED pattern improves in quality after a gentle anneal up to $\sim 150^\circ\text{C}$. Medium-energy backscattered electron-diffraction (MEED) patterns taken with an electron energy of 750 eV from a thick Cu overlayer showed a threefold symmetry in accordance with calculations using the single scattering cluster method^{8,16} for a Cu(111) face.¹⁷ An abrupt interface between the Cu overlayer and the TiO_2 substrate could clearly be distinguished by HRTEM; it is very sharp and well ordered.¹²

During evaporation of the Cu overlayer, the substrate XPS peaks do not change in shape or position. The binding energy of the Cu $2p_{3/2}$ photoelectrons decreases by 0.5 eV during the initial stages of the film growth (Fig. 4). The bulk value of the Cu binding energy is reached at a coverage corresponding to approximately one monolayer. The decrease of binding energy for the Cu $2p$ overlayer peak is of the same sign and magnitude as the one observed for the Cu $3d$ peak.⁵ Similar behavior has been observed for Cu on aluminum oxide.¹⁸ The shifts can be interpreted as due to emission from increasingly larger Cu clusters. Higher core-level binding energies are also observed for small metal clusters on inert substrates;¹⁹ e.g., Cu clusters and atoms isolated from each other in an inert matrix have been reported to exhibit a binding energy increased by 2.8 eV with respect to the bulk value.²⁰ We also note that no band bending due to Cu adsorption occurs, as indicated by the unchanged energy of the Ti $2p$ and O $1s$ features.

Sputtering the sample did not influence the growth

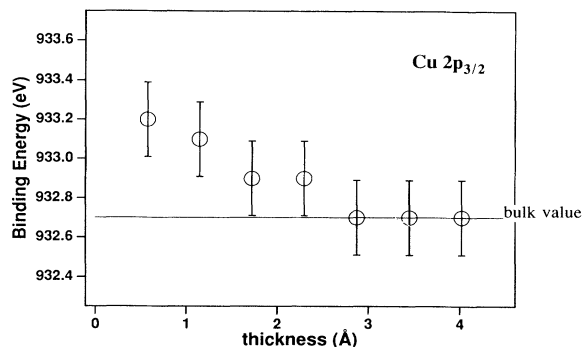


FIG. 4. The binding energy of the Cu $2p_{3/2}$ XPS signal for very low coverages of Cu on stoichiometric $\text{TiO}_2(110)$. The bulk value was obtained from a very thick Cu film (160 Å).

mode; in fact the results obtained from sputtered and annealed surfaces were quite similar. Again, the substrate and overlayer XPS signals show a smooth increase and decrease with Cu coverage, respectively. Figure 5 shows the integrated peak areas of the O $1s$ and Ti $2p$ signals (normalized to their respective values for an uncovered surface), and the Cu $2p_{3/2}$ signal [normalized to the value of a very thick (> 100 Å) Cu film]. Note that the sum of the (normalized) substrate and overlayer signals adds up to 1 over a wide range of coverages; the implications of this interesting observation will be discussed in Sec. IV B. The decrease of the LEIS substrate signal was comparable with that for evaporation onto a stoichiometric surface (Fig. 6). The experiments have been repeated and

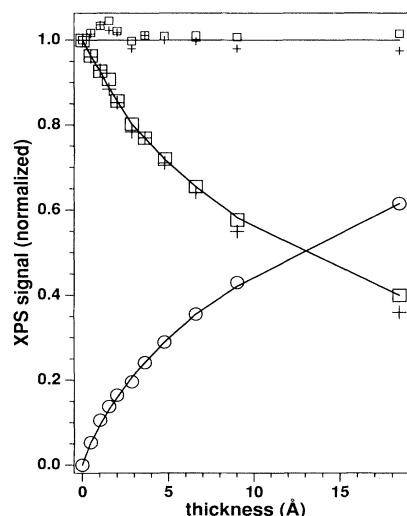


FIG. 5. XPS signals during Cu evaporation onto sputtered TiO_2 at room temperature. The Cu $2p_{3/2}$ signal (circles) has been normalized to the value of a very thick Cu film, the Ti $2p$ (squares) and O $1s$ (crosses) signals to the values of a clean surface, respectively. The small markers are the sums of the normalized overlayer and substrate values (crosses for oxygen and squares for titanium). The lines are drawn to guide the eye.

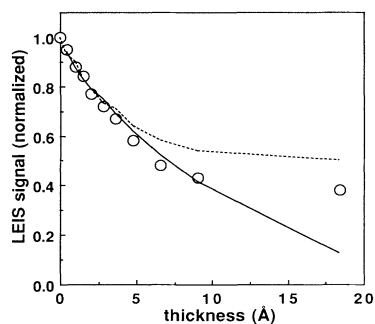


FIG. 6. The low-energy ion-scattering signal of titanium for Cu films on sputtered TiO_2 at room temperature. The lines represent calculations using the uniform layer model (broken line) and the hemispherical cap model (full line) as discussed in the text. The breaks in the calculated curves reflect the scattering in the XPS data which were used as input in the calculations.

reproduced several times on sputtered as well as annealed surfaces with no significant difference in the results.

B. Cu deposition onto TiO_2 at 160 K

The distinct cluster formation observed at room temperature must be connected with high mobility of the Cu atoms on the surface. In order to decrease the mobility of the adatoms, we performed evaporation onto an annealed cooled sample (160 K). Again, no breaks are visible in the XPS uptake curves. Even at a relatively high coverage of 27 Å, the substrate LEIS signals do not disappear completely but are attenuated to $\sim 80\%$ of the original value. Obviously, cooling the surface to a temperature of 160 K was not sufficient to inhibit diffusion and agglomeration of Cu atoms on the $\text{TiO}_2(110)$ surface. However, the diffusion process was slow enough to be observed within the time scale of the experiment: Figure 7 displays the XPS signals of the substrate and overlayer of a 27-Å-thick film, normalized to their respective values

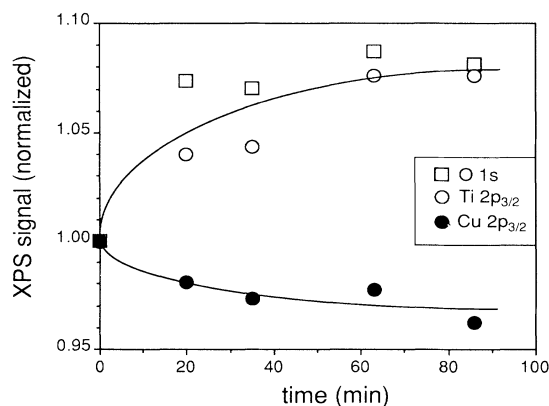


FIG. 7. The change of the XPS signals from 27-Å $\text{Cu}/\text{TiO}_2(110)$, with the annealing time at a sample temperature of 160 K.

immediately after evaporation. The signals show a noticeable change with time. The Cu signal decreases and both the Ti and O signals increase a few percent. No changes in the line shapes of any of the signals are observed.

C. Annealing effects

During annealing to higher temperatures, the XPS intensities change in the same direction as observed with increasing time at 160 K. Figure 8 shows the integrated peak area of $\text{Cu } 2p_{3/2}$ from 18-Å-thick overlayers versus annealing time. The initial evaporation was performed at room temperature. (Note that the $\text{Cu } 2p_{3/2}$ peak areas of the as-prepared films show little variation; the reproducibility of the thickness determination with the QCM is quite high.) The sample was then heated to the temperature indicated in Fig. 8 for a certain period of time, and the XPS spectra were taken after it cooled to room temperature again. The variation of the Cu signal shows the same qualitative behavior at all temperatures: a fast decrease at the beginning of the anneal and a steady-state condition characteristic of each annealing temperature.

No change in peak shape or position of either the Cu or the substrate signals takes place. If Cu diffused below the surface, one would expect electronic changes in the Cu or the substrate to be observable in XPS.

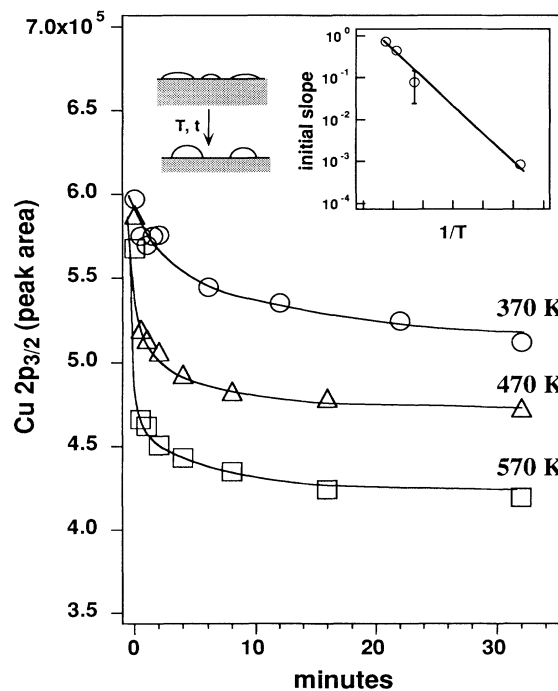


FIG. 8. $\text{Cu } 2p_{3/2}$ signals during annealing of 18-Å Cu films at different temperatures. The inset shows the initial slope of the curves; the coarsening of the clusters during annealing is sketched.

IV. DISCUSSION

A. Calculation of coverage and attenuation lengths

By combining the information from substrate and adsorbate LEIS and XPS signals with the average thickness d as determined from the (calibrated) QCM, we can give some estimate about the coverage (the fraction of the surface covered with Cu) and the cluster size of the Cu overlayer.

In order to make this estimate, we have to assume the geometry of the clusters. In the following discussion, we consider two cases: flat islands of arbitrary shape but uniform thickness [Figs. 9(a) and 9(b)], and isolated hemispherical caps with uniform radii [see Fig. 9(c)]. We further utilize the fact that we have five independent experimental signals (the average film thickness, and the substrate and overlayer signals from XPS and LEIS, respectively); this is far more than the number of parameters necessary for our calculations. We take a subset of the measured signals and calculate the parameters of the respective model. From the results, we calculate the values of the other subset and compare these with the experimental values. Thus we are able to estimate the validity of our approximations. This procedure assures that results from the simple models used will give meaningful information about the properties of the film.

B. The flat island model

First, consider that a fraction Θ of the surface is covered with islands of arbitrary shape and uniform thickness t [Fig. 9(a)],

$$d = \Theta t, \quad (1)$$

with d the average thickness determined from the QCM. Then the XPS intensities of the adsorbate and substrate signals, I_{ads} and I_{sub} , will follow:

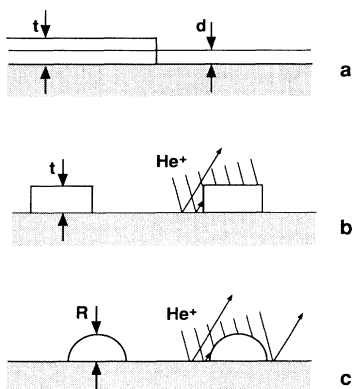


FIG. 9. Models used for the calculations. (a) Uniform layer with thickness t and coverage Θ ; d is the average thickness as determined from the quartz crystal monitor. (b) The macroscopic shadowing effect during LEIS. (c) Hemispherical caps with equal radius R ; macroscopic shadowing during LEIS is indicated.

$$\frac{I_{\text{ads}}}{I_{\text{ads}}(\infty)} = \Theta \left[1 - \exp \left[-\frac{t}{\lambda_{\text{ads}}} \right] \right], \quad (2)$$

$$\frac{I_{\text{sub}}}{I_{\text{sub}}(0)} = 1 - \Theta + \Theta \exp \left[-\frac{t}{\lambda_{\text{sub}}} \right], \quad (3)$$

with the intensities being normalized to the values of a thick ($d > 100 \text{ \AA}$) film, $I_{\text{ads}}(\infty)$, and an uncovered surface, $I_{\text{sub}}(0)$, respectively. From those normalized signals (see Fig. 5), Θ and t can be calculated.

λ_{ads} and λ_{sub} correspond to the attenuation length of the photoelectrons from the overlayer (kinetic energy of $\sim 500 \text{ eV}$ for Cu $2p_{3/2}$ excited with Al $K\alpha$) and the photoelectrons from the substrate passing through the Cu film, respectively. Either of the two substrate signals can be taken, since we observed no preferential coverage of oxygen or titanium, i.e., no favored site for Cu adsorption, and O $1s$ and Ti $2p$ kinetic energies are similar ($\sim 1000 \text{ eV}$).

Calculated and experimental values for inelastic mean free path lengths of electrons can be taken from the literature.^{21,22} However, we want to add a caveat. When using single-crystalline materials and an analyzer with a small acceptance angle, the attenuation length of photoelectrons can deviate dramatically from the inelastic mean free path length. Before proceeding with the calculations, we discuss this further.

Elastic scattering of electrons in a well-ordered single-crystalline matrix will give rise to forward focusing along close-packed crystal directions.²³ When adding an amorphous overlayer (or an overlayer with an epitaxial relationship different from the bulk) on top of the single crystal, “defocusing” will occur. If detection is done along a focusing direction, the electrons can be scattered elastically out of the acceptance angle of the analyzer by an overlayer film; this will effectively reduce the attenuation length. In our case, both O $1s$ as well as Ti $2p$ substrate photoelectrons exhibit forward focusing along the surface normal⁸ for sputtered as well as stoichiometric TiO₂(110). This is the direction along which the XPS signals have been recorded in our experiment. By adding the Cu overlayer, this forward focusing will be attenuated due to elastic scattering. The attenuation length λ_{sub} will comprise elastic- as well as inelastic-scattering contributions; it is expected that λ_{sub} will be smaller than the calculated inelastic mean free path length. For this reason, λ_{sub} was treated as a parameter in the calculations.

In Fig. 10, we plot the results of calculation of Θ and t from the Cu $2p_{3/2}$ peak areas [Eq. (2)] with $\lambda_{\text{ads}} = 8 \text{ \AA}$.^{21,24} The two groups of lines in Fig. 10 show the results for the normalized substrate signal calculated from Θ and t with different values for λ_{sub} . We have varied the values between 6 and 16 \AA , the latter being the calculated inelastic mean free path of 1000-eV electrons in Cu.²¹ The best fit is obtained for $\lambda_{\text{sub}} = 8 \text{ \AA}$, the same value as λ_{ads} .

The result that both attenuation lengths should be equal might seem surprising considering the difference in the kinetic energy. However, from the sum of the normalized XPS substrate and adsorbate signals (Fig. 10),

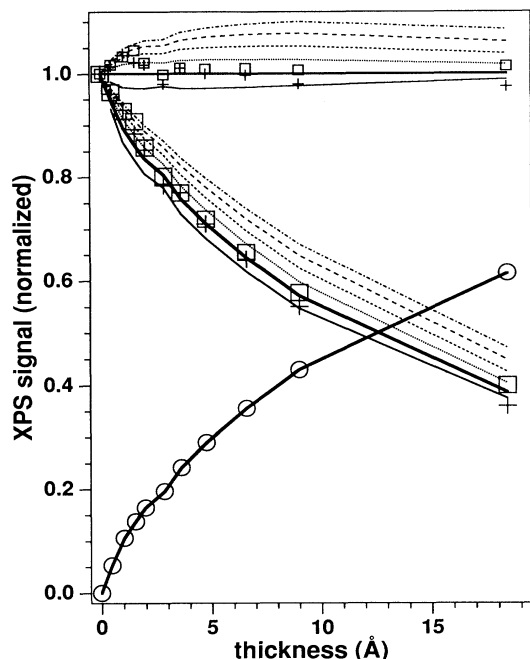


FIG. 10. XPS signals during Cu evaporation onto sputtered TiO_2 at room temperature (see Fig. 5). The lines are calculations using a uniform-layer model with variation of the attenuation length λ of the substrate XPS signals (thin solid line, $\lambda=6$ Å; thick solid line, $\lambda=8$ Å; \dots , $\lambda=10$ Å; $---$, $\lambda=12$ Å; $---$, $\lambda=14$ Å; $-\cdot-\cdot-$, $\lambda=16$ Å).

$\lambda_{\text{sub}} \cong \lambda_{\text{ads}}$ can readily be concluded: the normalized signals add up to 1 within a few percent for all coverages. Because of the complementary nature of Eqs. (2) and (3), the sum of the normalized substrate will depend on the relation between λ_{sub} and λ_{ads} ; e.g., if $\lambda_{\text{sub}} > \lambda_{\text{ads}}$, the sum should initially increase with increasing coverage. However, the absolute value will depend on the film thickness and shape. Only if $\lambda_{\text{sub}} \cong \lambda_{\text{ads}}$ will the sum be unity for all coverages. This is not only valid for the simple case of a uniformly thick film but for any morphology of the overlayer. [For the general case, imagine the surface being divided into infinitely small fractions Θ_i , each with a certain thickness t_i . Then Eqs. (2) and (3) consist of sums over the small fractions Θ_i . When adding both equations, the contributions from the substrate and the over-

$$\frac{I_{\text{ads}}}{I_{\text{ads}}(\infty)} = nR^2\pi - 2\pi n\lambda_{\text{ads}}^2 \left[1 - \left[1 + \frac{R}{\lambda_{\text{ads}}} \right] \exp \left[-\frac{R}{\lambda_{\text{ads}}} \right] \right], \quad (5)$$

$$\frac{I_{\text{sub}}}{I_{\text{sub}}(0)} = 1 - nR^2\pi + 2\pi n\lambda_{\text{sub}}^2 \left[1 - \left[1 + \frac{R}{\lambda_{\text{sub}}} \right] \exp \left[-\frac{R}{\lambda_{\text{sub}}} \right] \right]. \quad (6)$$

Again, if $\lambda_{\text{ads}} \sim \lambda_{\text{sub}}$, the sum of the normalized signals will be 1. (Remember that this is true in general, independent on the morphology of the overlayer.) We have used a value of 8 Å because of the considerations given above.

layer cancel out for each Θ_i and the sum will be unity again.]

Thus the sum of the (normalized) substrate and overlayer XPS signals can give valuable information. Because of the aforementioned large deviations of attenuation lengths from calculated inelastic mean free path lengths, this simple method should be regarded as helpful in obtaining information about the relationship of λ_{sub} and λ_{ads} .

Having determined the best fit for the attenuation lengths, we can proceed to calculate t and Θ from Eqs. (2) and (3). The results can be compared to the LEIS signals; e.g., the calculated uncovered fraction of the surface, $1 - \Theta$, can be compared to the attenuation of the normalized substrate signal for different Cu thicknesses. Because of the finite thicknesses of the clusters involved in our experiment, some ion trajectories will be blocked and will not reach the detector [Fig. 9(b)]. This macroscopic shadowing effect will strongly depend on the shape of the clusters but will generally lead to an overestimation of the coverage considering the LEIS signals alone, i.e., $1 - \Theta \geq I_{\text{sub}}^{\text{ion}} / I_{\text{sub}}^{\text{ion}}(0)$ has to be valid for all coverages and thicknesses.

The dotted line in Fig. 6 represents the results of the calculation. Despite the simple assumption of islands with uniform thickness, the calculated coverage values fit the LEIS data quite well for small coverages. With the increasing height of the islands, the macroscopic shadowing becomes stronger and the calculated curve in Fig. 6 deviates from the data for average thicknesses $d > 5$ Å.

C. The hemispherical cap model

We will now consider hemispherical caps with a single value of R [Fig. 9(c)]. Since the surface free energy of TiO_2 [0.28–0.38 J/m² (Ref. 25)] is much smaller than that of Cu [1.830 J/m² for Cu(111) (Ref. 26)] a hemispherical shape for the Cu clusters will be a reasonable assumption. Electron microscopy studies of metal films on MgO(001) corroborate this conjecture.²⁷

The radius R and the density n of the hemispheres can be calculated using the average thickness of the film, d (determined with the QCM),

$$d = \frac{2}{3}nR^3\pi \quad (4)$$

and the normalized XPS signals can be derived as

Including macroscopic shadowing at the hemispheres [Fig. 9(c)], the LEIS signal from the substrate should follow

$$\frac{I_{\text{sub}}^{\text{ion}}}{I_{\text{sub}}^{\text{ion}}(0)} = 1 - \frac{3}{2}nR^2\pi \quad (7)$$

for our scattering geometry. Here the situation was simplified further by assuming that the neutralization of the He^+ ions does not change with coverage, i.e., that the decrease in the substrate LEIS signals is caused by a coverage with Cu atoms and macroscopic shadowing only. The assumption of unchanged neutralization might be justified when the covered and uncovered areas are big enough so that the local electronic structure is not significantly changed by a neighboring area with a very different electronic structure.

Figure 11 shows the results of a calculation of the radius and density of the hemispheres for evaporation onto the sputtered surface using the XPS adsorbate signal and d . Because $\lambda_{\text{ads}} \sim \lambda_{\text{sub}}$, Eqs. (5) and (6) are no longer linearly independent and either one can be used. We have chosen the adsorbate signal because it has the higher absolute count rate (Fig. 1).

Again, the quality of the fit can be controlled by comparing the calculated LEIS intensities with experimental data (the solid line in Fig. 6). The assumption of hemispherical caps describes the data better than the above-described model of islands with uniform thickness. For an average thickness above 10 Å, more than half of the sample is covered and the assumption of hemispheres isolated from each other is no longer valid. This explains the decrease in the calculated cluster density (Fig. 11) and the deviation from the experimental data for higher thicknesses in Fig. 6.

D. Annealing and diffusion

The behavior of the XPS signals with annealing can be explained by a change in the morphology of the copper films. An increase in cluster height will increase the attenuation of the copper photoelectrons within the clusters and decrease the Cu $2p_{3/2}$ signal intensity. If the shape change is accompanied by an increase in exposed substrate area, the intensity of the substrate Ti and O signals will be increased. A "rounding" of the clusters would affect the XPS signals in such a way (see the inset in Fig. 8); this rounding will be driven by upward hopping of Cu atoms at steps and by self-diffusion along the planes of the cluster.

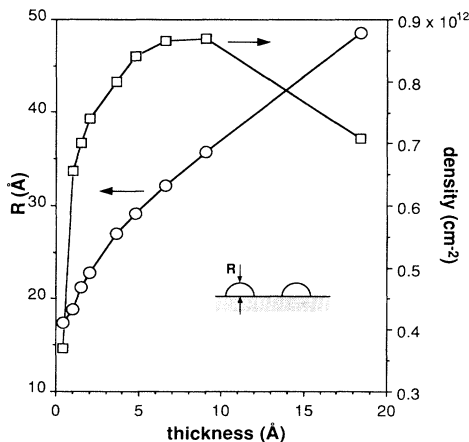


FIG. 11. Radius and density of the copper clusters calculated assuming a hemispherical cap model.

Additionally, single Cu atoms which are dispersed on the surface might migrate toward the clusters and subsequently be incorporated. Bigger clusters could be formed out of smaller ones ("Ostwald ripening"), either if the small clusters are mobile enough to merge together or if single atoms break away and move toward bigger clusters.

The relative contributions of all the processes which give rise to the change in the film morphology are hard to distinguish. Since we lack a microscopic picture of the annealing process, a quantitative estimate about an activation energy extracted from the macroscopic information has to be taken with some caution. By plotting the initial rate of change of the Cu $2p_{3/2}$ signal in an Arrhenius plot (Fig. 8), an activation energy of 0.13 eV was obtained. This number represents the activation energy for the rate-limiting step of the process which gives rise to the observed changes in the XPS signals. Generally the activation energy for diffusion will be on the order of 5–20% of the binding energy of an atom to a surface. The diffusion barrier on Cu surfaces is very low, as shown by Hansen *et al.*²⁸ However, the small activation energy of the process observed can be taken as an indication of the weak interaction between Cu and $\text{TiO}_2(110)$ (see below).

We modeled the change in coverage and cluster size using the hemispherical cap model discussed in Sec. IV C. During annealing, the mean radius of the hemispheres increases; e.g., we estimate an increase in the radius from 50 to 65 Å for the equilibrium reached after 20 min at 570 K. For higher coverages, LEED patterns of the hexagonal Cu overlayer and the (annealed) $\text{TiO}_2(110)$ substrate appear simultaneously; considering that the surface has to be ordered within the coherence length of the LEED electrons (~ 100 Å), the estimate of the cluster size does not seem to be too unrealistic.

E. Interpretation and trends

All our experimental results, i.e., the Volmer-Weber growth at low substrate temperatures, no or very weak influence of the surface defect densities on the nucleation behavior, and the low activation barrier for diffusion, are consistent with a very weak interaction between Cu and the TiO_2 substrate. The weak bond between metal and metal oxide is connected with a lack of electron transfer from the metallic overlayer to the substrate. No oxidation of Cu was observed in this study; the change in the binding energy of the Cu $2p_{3/2}$ electrons for low coverages can be attributed to finite cluster size effects. Systems in which a stronger bond is observed usually imply that the overlayer metal atom is oxidized due to interaction with the lattice oxygen. This is seen in the case of Fe and Cr overlayers on TiO_2 ; correlated with this is the more complete wetting behavior of the adsorbed metal.^{7,29} Oxidation of the overlayer metal will be accompanied by a reduction of the substrate cations.

No change in the oxidation state of the Ti^{4+} or the O^{2-} substrate ions is observed with XPS for Cu overlayers. This is in agreement with molecular orbital calculations by Anderson and co-workers^{30,31} which showed

that O^{2-} ions on an oxide surface are not able to form a strong covalent bond with the metal adatom. A stronger bond can only be formed when a part of the electron density at the oxygen ions is contributed by the metal overlayer.

The relative oxygen affinities of the overlayer and the substrate metals can be used to predict the possibility of an oxidation-reduction reaction, as pointed out by Zhang and Henrich.³² Overlayer oxidation is observed for reactive metals such as Ti,³³ V,³² Fe,^{7,34} and Cr,⁷ but weak interaction is observed for Pt (Ref. 35) and Rh.³⁵⁻³⁷ Systematic studies of 3d metal overlayers for other oxide materials show similar trends across the Periodic Table: A reduction in shear strength of metal-sapphire contacts,³⁸ and a reduction in bond strength between close-packed metals and the (0001) α -Al₂O₃ surface.³⁹

The reactivity toward oxygen also strongly influences the growth mode of an ultrathin metal film; a systematic trend in the growth mode of 3d metals on tungsten oxide was observed recently.⁴⁰ In the case of a TiO₂(110) substrate, the nonwetting behavior of Cu can be correlated with its low reactivity against oxygen.

V. SUMMARY

Cu shows very weak interaction with a TiO₂ surface. At low temperatures (160 K), as well as at room tempera-

ture, Volmer-Weber growth is observed on the TiO₂(110) surface. Even at relatively high average coverages (> 30 Å), a substantial fraction (> 30%) of the substrate is uncovered. The clusters exhibit a (111) orientation. Creation of substrate defects by Ar⁺ sputtering prior to Cu deposition does not influence the observed growth behavior.

At low temperature (160 K), diffusion of Cu can be observed within the time scale of the experiment. During annealing to moderate temperatures, the size of the clusters increases and an increase in the uncovered fraction of the sample is observed. The activation energy for the diffusion process has been determined as ~0.13 eV.

Two models were used to fit the data. The best fit was obtained for a simple hemispherical model for the shape of the clusters; their radius has been estimated to be on the order of tens of angstroms. The size of the clusters increases with increasing Cu doses, and the density is ~10¹² cm⁻².

ACKNOWLEDGMENTS

The authors acknowledge valuable discussions with E. Garfunkel. This work was supported in part by the National Science Foundation, Grant No. DMR-8907553.

- ¹E. Bauer, Z. Kristallogr. Kristallgeom. Krystallphys. Kristallchem. **110**, 372 (1959).
- ²W. Göpel, J. A. Anderson, S. Frankel, M. Jaehnig, K. Phillips, J. A. Schäfer, and G. Rucker, Surf. Sci. **139**, 333 (1984).
- ³V. E. Henrich, in *Surface and Near-Surface Chemistry of Oxide Materials*, edited by J. Nowotny and L.-C. Dufour (Elsevier, Amsterdam, 1985).
- ⁴P. J. Møller and M.-C. Wu, Surf. Sci. **224**, 265 (1989).
- ⁵P. J. Møller and M.-C. Wu, Surf. Sci. **224**, 250 (1989).
- ⁶J.-M. Pan and T. E. Madey, J. Vac. Sci. Technol. (to be published).
- ⁷J.-M. Pan, L. Zhang, U. Diebold, and T. E. Madey (unpublished).
- ⁸B. L. Maschhoff, J.-M. Pan, and T. E. Madey, Surf. Sci. **259**, 190 (1991).
- ⁹J.-M. Pan, U. Diebold, B. L. Maschhoff, and T. E. Madey, J. Vac. Sci. Technol. A **10**, 2470 (1992).
- ¹⁰P. A. Thiel and T. E. Madey, Surf. Sci. Rep. **7**, 211 (1987).
- ¹¹D. C. Cronemeyer, Phys. Rev. **87**, 876 (1952).
- ¹²P. Lu and F. Cosandey (unpublished).
- ¹³C. Argile and G. E. Rhead, Surf. Sci. Rep. **10**, 277 (1989).
- ¹⁴U. Bardi, Appl. Surf. Sci. **51**, 89 (1991).
- ¹⁵B. V. King, D. J. O'Connor, Y. Shen, R. J. MacDonald, M. Katayama, and M. Aono, Appl. Surf. Sci. **48/49**, 246 (1991).
- ¹⁶D. J. Friedman and C. S. Fadley, J. Electron Spectrosc. **51**, 689 (1990).
- ¹⁷B. L. Maschhoff (private communication).
- ¹⁸V. D. Castro, G. Polzonetti, and R. Zanoni, Surf. Sci. **162**, 348 (1985).
- ¹⁹W. F. Egelhoff, Surf. Sci. Rep. **6**, 253 (1987).
- ²⁰D. Schmeisser, K. Jacobi, and D. M. Kolb, J. Chem. Phys. **75**, 5300 (1981).
- ²¹S. Tanuma, C. J. Powell, and D. R. Penn, Surf. Interf. Anal. **11**, 577 (1988).
- ²²W. Dolinski, S. Mróz, and M. Zagórski, Surf. Sci. **200**, 361 (1988).
- ²³C. S. Fadley, in *Synchrotron Radiation Research: Advances in Surface Science*, edited by R. Z. Bachrach (Plenum, New York, 1990).
- ²⁴H. Ebel, C. Pöhn, R. Svagera, M. E. Wernerle, M. F. Ebel, and A. Jablonski, J. Electron Spectrosc. Relat. Phenom. **50**, 109 (1990).
- ²⁵S. H. Overbury, P. A. Bertrand, and G. A. Somorjai, Chem. Rev. **75**, 547 (1975).
- ²⁶J. R. Smith and A. Banerja, Phys. Rev. Lett. **59**, 2451 (1987).
- ²⁷K. Takayanagi, K. Yagi, and G. Honjo, Thin Solid Films **48**, 137 (1978).
- ²⁸L. Hansen, P. Stolze, K. W. Jakobsen, and J. K. Nørskov, Phys. Rev. B **44**, 6523 (1991).
- ²⁹U. Diebold, J.-M. Pan, and T. E. Madey, Surf. Sci. (to be published).
- ³⁰A. B. Anderson and S. P. Mehandru, J. Electrochem. Soc. **132**, 1695 (1985).
- ³¹A. B. Anderson, C. Ravimohan, and S. P. Mehandru, Surf. Sci. **183**, 438 (1987).
- ³²Z. Zhang and V. E. Henrich, Surf. Sci. **277**, 263 (1992).
- ³³G. Rucker and W. Göpel, Surf. Sci. **181**, 530 (1987).
- ³⁴J. Deng, D. Wang, X. Wei, R. Zhai, and H. Wang, Surf. Sci. **249**, 213 (1991).
- ³⁵K. Tamura, M. Kudo, M. Owari, and Y. Nihei, Chem. Lett. **1986**, 1921.
- ³⁶D. N. Belton, Y.-M. Sun, and J. M. White, J. Phys. Chem. **88**, 1690 (1984).
- ³⁷D. N. Belton, Y. M. Sun, and J. M. White, J. Phys. Chem. **88**, 5172 (1984).
- ³⁸S. V. Pepper, J. Appl. Phys. **47**, 801 (1976).
- ³⁹K. Nath and A. B. Anderson, Phys. Rev. B **33**, 1013 (1989).
- ⁴⁰C. H. F. Peden, K. B. Kidd, and N. D. Shinn, J. Vac. Sci. Technol. A **9**, 1518 (1991).